

RESEARCH ARTICLE | MAY 05 2023

Resonant adhesion structure makes negative acoustic radiation force

Gong Menyang (宫门阳); Shi Minji (施敏吉); Li Yuanyuan (李媛媛); ... et. al



Physics of Fluids 35, 057108 (2023)

<https://doi.org/10.1063/5.0150180>

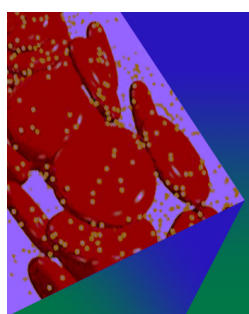


View
Online



Export
Citation

CrossMark



Physics of Fluids

Special Topic: Flow and Forensics

Submit Today!

AIP
Publishing

Resonant adhesion structure makes negative acoustic radiation force

Cite as: Phys. Fluids 35, 057108 (2023); doi: 10.1063/5.0150180

Submitted: 13 March 2023 · Accepted: 22 April 2023 ·

Published Online: 5 May 2023



View Online



Export Citation



CrossMark

Menyang Gong (宫门阳),¹ Minji Shi (施敏吉),² Yuanyuan Li (李媛媛),¹ Xin Xu (徐鑫),¹ Zhonghan Fei (费仲晗),¹ Yupei Qiao (乔玉配),³ Jiehui Liu (刘杰惠),¹ Aijun He (何爱军),^{4,a)} and Xiaozhou Liu (刘晓宙),^{1,5,a)}

AFFILIATIONS

¹Key Laboratory of Modern Acoustics, Institute of Acoustics and School of Physics, Collaborative Innovation Center of Advanced Microstructures, Nanjing University, Nanjing 210093, China

²Aston Institute of Photonic Technologies, Aston University, Birmingham B4 7ET, United Kingdom

³School of Physics and Electronic Science, Guizhou Normal University, Guiyang 550001, China

⁴School of Electronic Science and Engineering, Nanjing University, Nanjing 210023, China

⁵State Key Laboratory of Acoustics, Institute of Acoustics, Chinese Academy of Sciences, Beijing 100190, China

^{a)}Authors to whom correspondence should be addressed: haj@nju.edu.cn and xzliu@nju.edu.cn

ABSTRACT

Previously, the design of negative acoustic radiation force was mostly based on beam control. Realizing the negative acoustic radiation force through the design of the manipulated structure is a new and valuable idea. In this paper, a resonant adhesion structure capable of generating negative acoustic radiation force is designed. Finite element simulations are carried out to verify the feasibility of this negative acoustic radiation force scheme. The variation law of the acoustic radiation force with the frequency of the incident acoustic beam and various parameters of the resonant adhesion structure is explored and explained in detail. The proposal of this design lays a foundation for the realization of the negative acoustic radiation force, which has broad application prospects in the fields of medicine and life sciences.

Published under an exclusive license by AIP Publishing. <https://doi.org/10.1063/5.0150180>

I. INTRODUCTION

As an important acoustic nonlinear effect, the acoustic radiation force (ARF) in fluid media has been widely used in medicine and life sciences.^{1–5} The application of ARF in fluid has also received extensive attention.^{6–9} ARF is a non-contact technology that can transmit momentum to particles or biological tissues in fluids, so as to realize their manipulation. After the optical tweezers won the Nobel Prize, the acoustic tweezers also became a research hotspot.^{2,10–12} The ARF, being the principle behind the acoustic tweezers, has attracted widespread attention in recent years.^{13–18} Compared to the optical force, the ARF has many advantages such as better biocompatibility and lower thermal effects, which is quite suitable for applications in fluid media. The ARF experienced by standard particles such as spherical particles or cylindrical particles in various acoustic fields has been extensively studied.^{10,19–30} Under the traditional design, the generally obtained ARF is manifested as positive, which has caused many restrictions on the application. This means that sound sources need to be added on both sides of the target particle. Therefore, the proposal of negative ARF is an important complement to the complete

solution of the ARF. At present, the negative ARF is mainly realized by beam control, such as designing non-diffracting sound beams or suppressing backscattering.^{4,31–36} These methods require relatively harsh conditions of use and have considerable limitations. Few people have taken the structure of the transported object as the research direction for the realization of negative ARF until now. However, in medicine and life sciences, the design of the structure of the transported object is feasible. Therefore, it is quite meaningful to study and expand the new mechanism of realizing the negative ARF. In this work, a resonant adhesion structure is designed, which can exhibit a negative ARF externally in a general acoustic field. Based on this structure, not only the manipulation, recognition, and transfer of particles can be realized in the fields of medicine and life sciences, but also some interesting applications can be realized, such as acoustic pixel display.

II. THEORY

Based on the definition, the expression of the ARF on a general structure can be expressed as³⁰

$$\begin{aligned} F = \iint_s (p - p_0) \mathbf{n} ds &= \iint_s \rho_0 \left(\frac{\partial \Phi_{\text{tol}}}{\partial t} \right) \mathbf{n} ds \\ &+ \iint_s \frac{1}{2} \rho_0 \left(\frac{\partial \Phi_{\text{tol}}}{\partial z} \right)^2 \mathbf{n} ds \\ &- \iint_s \frac{1}{2} \frac{\rho_0}{c_0^2} \left(\frac{\partial \Phi_{\text{tol}}}{\partial t} \right)^2 \mathbf{n} ds. \quad (1) \end{aligned}$$

Here, $p - p_0$ is the sound pressure, z is the propagation direction of the incident sound beam, \mathbf{n} is the unit direction vector in the z direction, ρ_0 is the density of the environment medium, c_0 is the sound velocity in the environment medium, and Φ_{tol} is the velocity potential of the total sound field including the incident sound field and the scattered sound field.

The resonant adhesion structure and the auxiliary resonant structure are designed as shown in Fig. 1. The periodic structures above is the resonant adhesion structure, while the structure below is the auxiliary resonant structure. The incident sound wave is emitted from the auxiliary resonant structure, forming the incident sound field from bottom to top. In the magnified view of the upper structure, a_1 , a_2 , a_3 , and a_4 represent the width of the unit of the resonant adhesion structure, the width of the gap between the two units of the resonant adhesion structure, the thickness of the unit of the resonantly adhered structure, and the width of the gap between the resonant adhesion structure and the auxiliary resonant structure, respectively.

Under normal circumstances, if there is no participation of the auxiliary resonant structure, the resonant adhesion structure will be subject to the positive ARF with the same direction as the incident sound, as shown by F_1 in Fig. 1. Due to the introduction of the auxiliary resonant structure, the resonant adhesion structure and the auxiliary resonant structure form a resonant cavity, resulting in the multiple scattering. This multiple scattering greatly changes the

scattering field around the resonant adhesion structure, which enables the inversion of the ARF, as shown by F_2 in Fig. 1.

Therefore, as shown in Fig. 1, the resonant adhesion structure is designed to store energy to release the negative momentum, which enables it to realize the negative ARF in a simple sound field. The multiple scattering in the cavity could produce a pulling force on the unit of the resonant adhesion structure, which is verified by the following formulation simulation.

The sound field in the scattering part depends on the boundary conditions, so adjusting the boundary conditions could be an important method to adjust the momentum transport.

III. FORMULATION SIMULATION VERIFICATION

In order to verify that the resonant adhesion structure can indeed generate a negative ARF, the finite element simulations are carried out. The software used for the finite element simulation is COMSOL 6.1. The mesh size of the finite element simulation is limited by the wavelength, and the maximum grid size does not exceed one-sixth of the wavelength. Both the resonant adhesion structure and the auxiliary resonant structure are made of aluminum. The environmental medium is water. The material parameters are shown in Table I, which will be used below unless otherwise specified. In order to avoid the influence of the limited number of repeating structure units on the ARF, the number of units of the resonant adhesion structure is selected as $n = 9$. If the resonant adsorption structure is infinitely extended, due to the symmetry of the structure, each unit of the whole resonant adhesion structure is equivalent. So the ARF acting on each unit is exactly the same. The ARF will only move the entire resonant structure up and down without changing the relative position between units. So that the middlemost unit of the resonant adhesion structure is selected to calculate the ARF it receives.

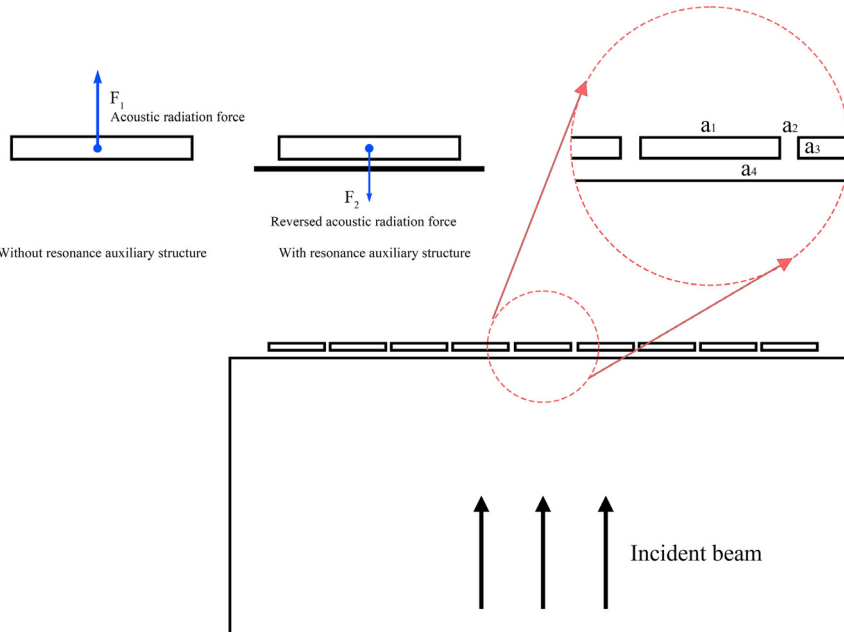


FIG. 1. Schematic diagram of the resonant adhesion structure and the auxiliary resonant structure.

TABLE I. Parameter selection of the resonant adhesion structure, the auxiliary resonant structure, and the environmental medium.

Parameter	Symbols	Numerical value
Density of aluminum	ρ_1	$2.7 \times 10^3 \text{ kg/m}^3$
Poisson's ratio of aluminum	ν_1	0.33
Sound speed of aluminum	c_1	6300 m/s
Density of water	ρ_2	$1.0 \times 10^3 \text{ kg/m}^3$
Sound speed of water	c_2	1480 m/s
The width of the unit of the resonant adhesion structure	a_1	0.4 mm
The width of the gap between the two units of the resonant adhesion structure	a_2	0.05 mm
The thickness of the unit of the resonant adhesion structure	a_3	0.05 mm
The width of the gap between the resonant adhesion structure and the auxiliary resonant structure	a_4	0.02 mm

A. Variation law of acoustic radiation force with frequency spectrum of incident sound wave

First, the variation of the ARF with the frequency of the incident acoustic wave is studied. As shown in Fig. 2, the direction of the ARF on the units of the resonant adhesion structure is reversed near 12.81 MHz. At this point, the pushing force that pushes the resonant adhesion structure away from the auxiliary resonant structure is changed to a pulling force that pulls the resonant adhesion structure to the auxiliary resonant structure.

To further illustrate the appearance of the pulling force, the spatial distribution of the sound pressure is plotted as shown in Fig. 3. Figures 3(a)–3(f) depict the sound pressure distributions when the incident sound frequency is 10, 11, 12, 13, 14, and 15 MHz, respectively. Figure 3(g) depicts the sound pressure distribution when the frequency of the incident sound wave is 12.81 MHz, where the ARF

obtains a negative maximum value. Figure 3(h) depicts an enlarged image of Fig. 3(g), showing the sound field distribution near the most central unit of the resonant adhesion structure. It can be seen that with the impact of the resonant sound field, the unit experiences an obvious pulling force. Figure 3(i) depicts an enlarged image of Fig. 3(e), showing the sound field distribution when the ARF affected upon the unit of the resonant adhesion structure has turned to positive. It can be seen that with the impact of the resonant sound field, the unit is subject to an obvious pushing force.

B. Variation law of acoustic radiation force with the width of the unit of the resonant adhesion structure

The reason for selecting these incident frequencies is to achieve resonance in the resonant cavity. Therefore, the wavelength of the incident acoustic wave should be in the same order of magnitude as the thickness of the cavity. As shown in Fig. 2, the peak of the negative ARF occurs around 12.81 MHz in this structure. So, in order to better illustrate the mechanism, 10, 13, and 15 MHz are selected as examples in the following finite element simulations.

The variation of the ARF with the width of the unit of the resonant adhesion structure is studied. As shown in Fig. 4, when the frequency of the incident acoustic beam is 10, 13, and 15 MHz, the resonant adhesion structure can obtain a negative ARF at an appropriate value of a_1 . This provides a parametric dimension for the design of units of resonant adhesion structures. It can be seen that as the frequency increases, the reverse peak value gradually decreases. However, when the frequency is large, multiple reverse peaks may appear. For example, when the frequency of incident wave is 15 MHz, there are two a_1 parameters to realize the negative ARF. This is because the incident waves of different frequencies form different resonance situations in the cavity with different values of a_1 . This leads to different multiple scattering in the near field as shown in Fig. 5. Therefore, when the parameters are selected properly, the direction of the ARF is reversed. In general, all of these resonant peaks can be used to design negative ARF schemes. The parameter a_1 will affect the width of the resonant cavity, thereby affecting the occurrence and amplitude of resonance in the resonant cavity, and then affecting the amplitude and the number of peaks of the negative ARF.

To illustrate the sound field distribution in more detail, the spatial distribution of the sound pressure is plotted as shown in Fig. 5. Figures 5(a)–5(c), respectively, show the sound pressure distribution when the width of the unit of the resonant adhesion structure is 0.3 mm and the frequency of the incident sound wave is 10, 13, and 15 MHz. For the incident sound waves of these three frequencies, the units of the resonant adhesion structure are all subject to forward ARFs. Figures 5(d)–5(f), respectively, show the sound pressure distribution when the width of the unit of the resonant adhesion structure is 0.4 mm and the frequency of the incident sound wave is 10, 13, and 15 MHz. Only for the incident sound wave at the frequency of 13 MHz, the unit of the resonant adhesion structure experiences a negative ARF. With the impact of the incident sound waves of the other two frequencies, the unit of the resonant adhesion structure is subject to the forward ARF. Figures 5(g)–5(i), respectively, show the sound pressure distribution when the width of the unit of the resonant adhesion structure is 0.5 mm and the incident sound wave frequency is 10, 13, and 15 MHz. For the incident sound waves of these three frequencies, the units of the resonant adhesion structure all experience

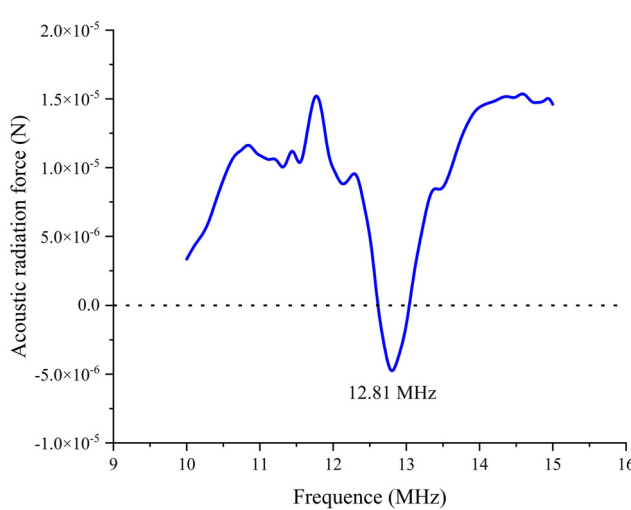


FIG. 2. Variation of the ARF with the frequency of the incident acoustic wave.

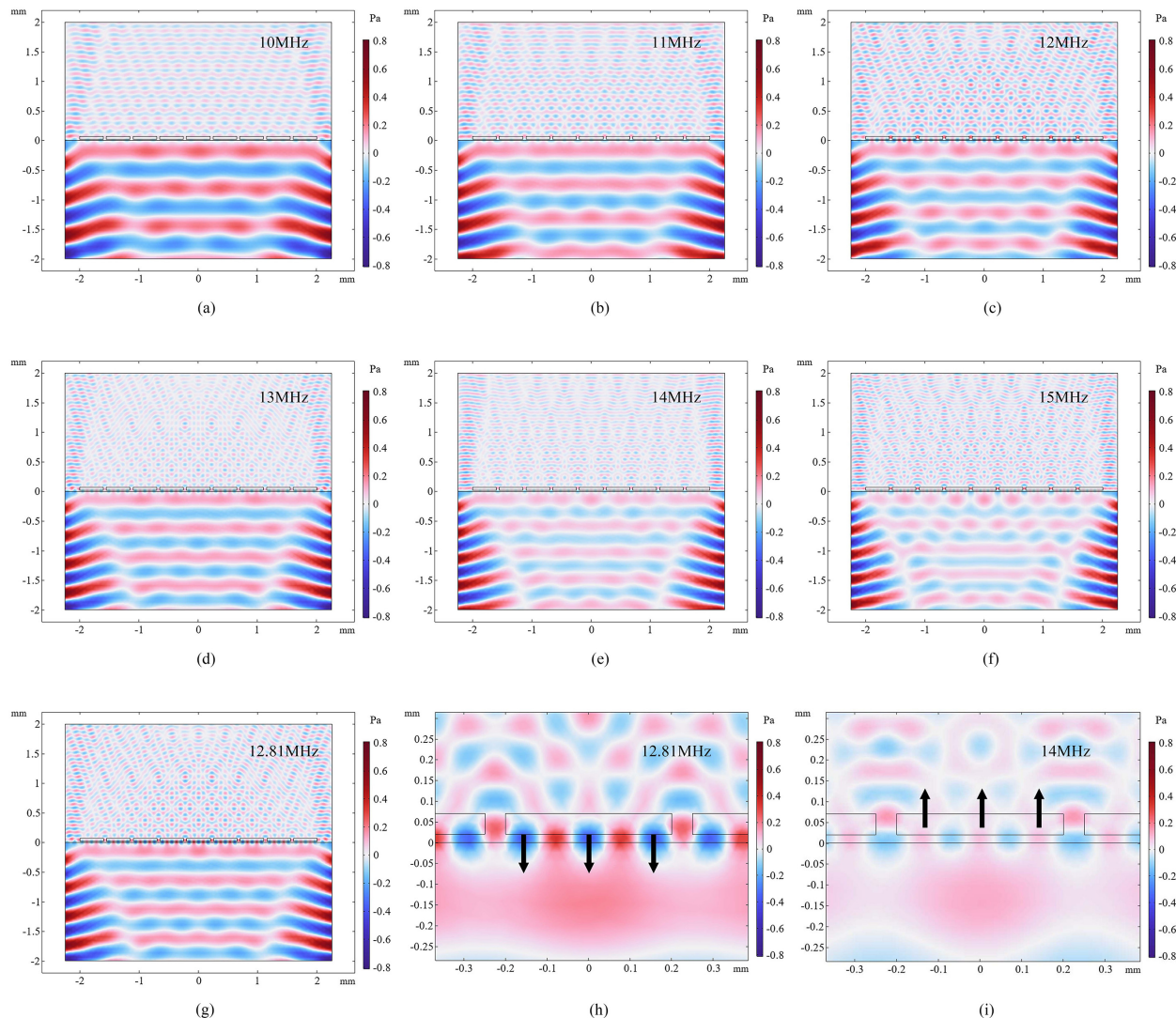


FIG. 3. Sound pressure distributions with an incident sound wave at a frequency of (a) 10, (b) 11, (c) 12, (d) 13, (e) 14, (f) 15, (g) 12.81, (h) 12.81, and (i) 14 MHz.

forward ARFs. Based on this, the width of the unit of the resonant adhesion structure can be designed to accommodate different incident beams. Likewise, the frequency of the incident beam can be adjusted to control the direction of the ARF experienced by the resonant adhesion structure with different width of the unit.

C. Variation law of acoustic radiation force with the width of the gap between the two units of the resonant adhesion structure

The variation of the acoustic radiation force with the width of the gap between the two units of the resonant adhesion structure is studied. As shown in Fig. 6, only when the frequency of the incident acoustic beam is near 13 MHz, the resonant adhesion structure can obtain a

negative ARF at the appropriate value of a_2 . This also provides a parametric dimension for the design of the units of the resonant adhesion structure. The influence of a_2 on the ARF is more manifested in its control of the boundary conditions of the resonant cavity. Different parameter conditions bring different resonance situations. When the frequency is too high or too low, different multiple scattering in the near field can be formed in the cavity, which is also confirmed by the results of sound field distribution in Fig. 7.

To illustrate the sound field distribution in more detail, the spatial distribution of the sound pressure is plotted as shown in Fig. 7. Figures 7(a)–7(c), respectively, depict the sound pressure distribution when the width of the gap between the two units of the resonant adhesion structure is 0.04 mm and the frequency of the incident sound wave is 10, 13, and 15 MHz. With the impact of the incident sound

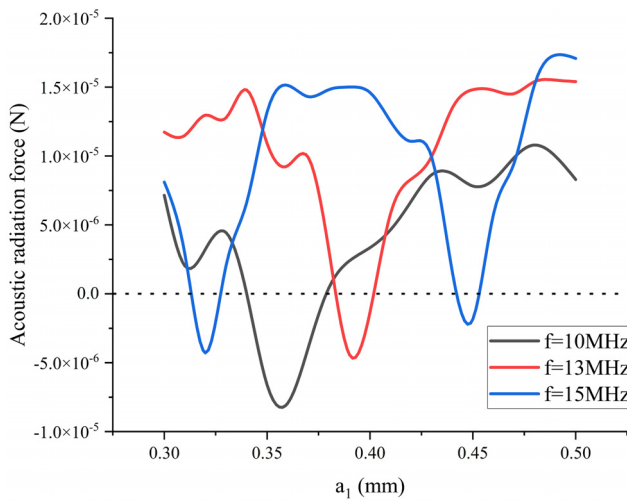


FIG. 4. Variation of the ARF with the width of the unit of the resonant adhesion structure.

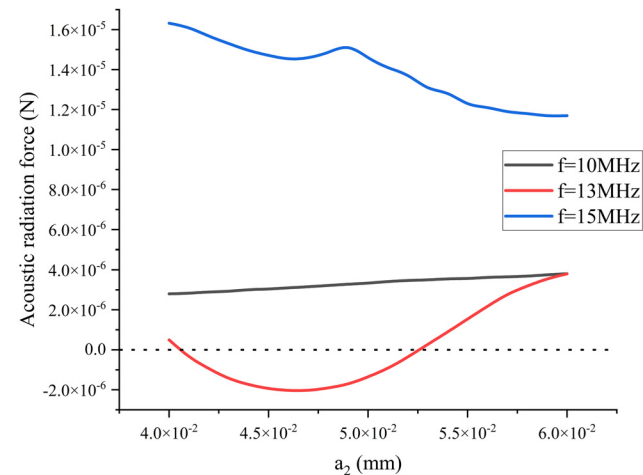


FIG. 6. Variation of the ARF with the width of the gap between the two units of the resonant adhesion structure.

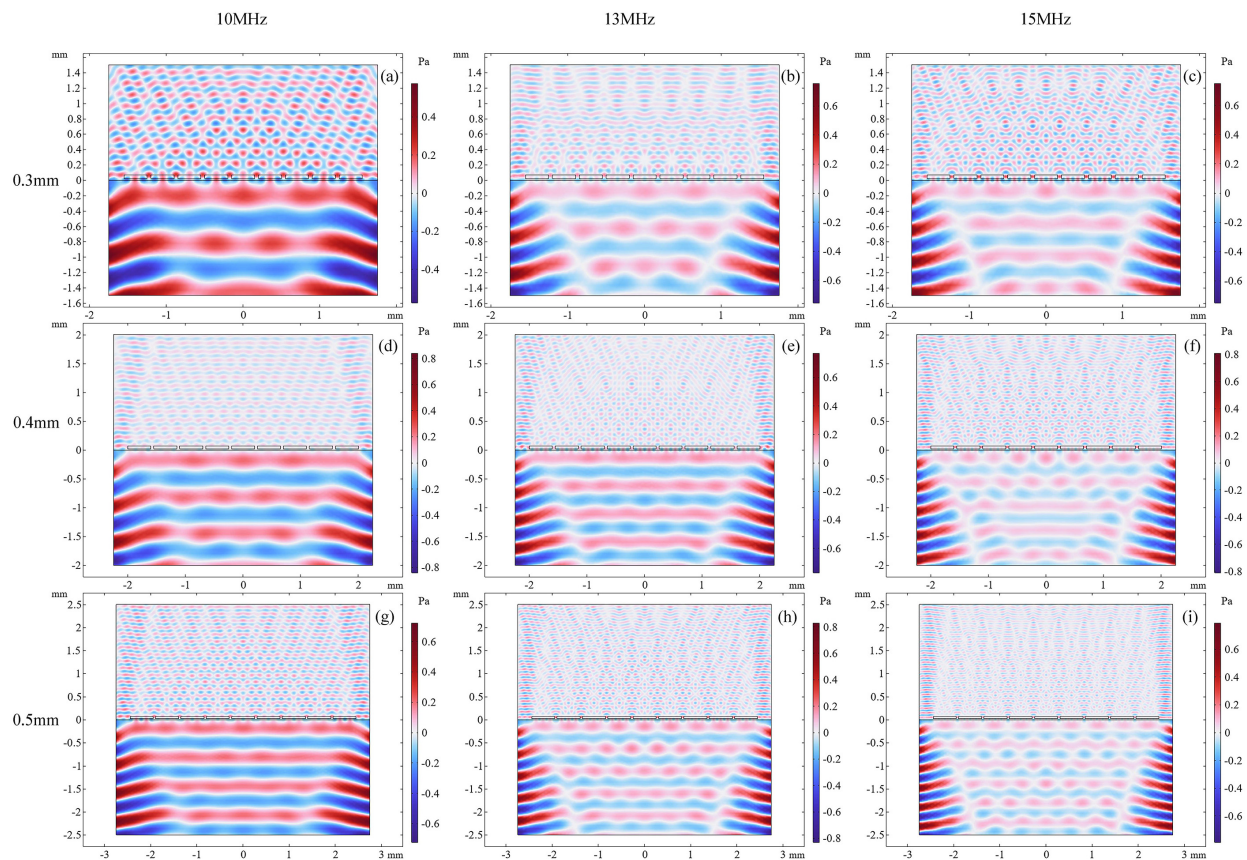


FIG. 5. Sound pressure distributions when the frequency of the incident sound wave and the width of the unit of the resonant adhesion structure are (a) 10 MHz , 0.3 mm ; (b) 13 MHz , 0.3 mm ; (c) 15 MHz , 0.3 mm ; (d) 10 MHz , 0.4 mm ; (e) 13 MHz , 0.4 mm ; (f) 15 MHz , 0.4 mm ; (g) 10 MHz , 0.5 mm ; (h) 13 MHz , 0.5 mm ; and (i) 15 MHz , 0.5 mm .

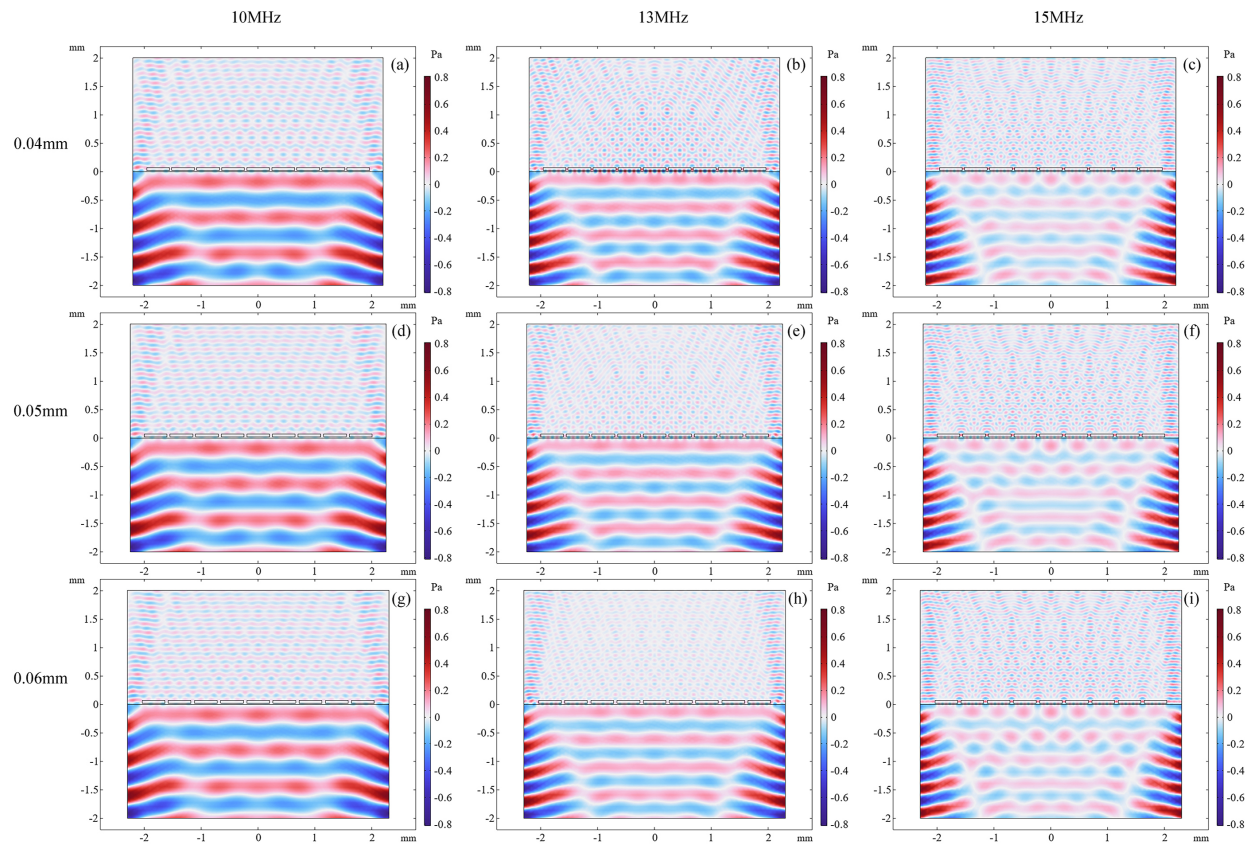


FIG. 7. Sound pressure distributions when the frequency of the incident sound wave and the width of the gap between the two units of the resonant adhesion structure are (a) 10 MHz, 0.04 mm; (b) 13 MHz, 0.04 mm; (c) 15 MHz, 0.04 mm; (d) 10 MHz, 0.05 mm; (e) 13 MHz, 0.05 mm; (f) 15 MHz, 0.05 mm; (g) 10 MHz, 0.06 mm; (h) 13 MHz, 0.06 mm; and (i) 15 MHz, 0.06 mm.

waves of these three frequencies, the units of the resonant adhesion structure are all subject to forward ARFs. Figures 7(d)–7(f), respectively, depict the sound pressure distributions when the width of the gap between the two units of the resonant adhesion structure is 0.05 mm and the frequency of the incident sound wave is 10, 13, and 15 MHz. Only for the incident sound wave at the frequency of 13 MHz, the unit of the resonant adhesion structure experiences a negative ARF. For the incident sound waves of the other two frequencies, the unit of the resonant adhesion structure is subject to a forward ARF. Figures 7(g)–7(i), respectively, depict the sound pressure distributions when the width of the gap between the two units of the resonant adhesion structure is 0.06 mm and the frequency of the incident sound wave is 10, 13, and 15 MHz. With the impact of the incident sound waves of these three frequencies, the units of the resonant adhesion structure all experience forward ARFs. The gap between the two units of the resonant adhesion structure is also an important factor in regulating the ARF affected on each unit. In some cases, the ARF can reverse due to change of the gap. This offers an idea that the direction of the ARF could be controlled by non-acoustic parameters such as electromagnetic interference and temperature, which can affect the gap between the two units.

D. Variation law of acoustic radiation force with the thickness of the unit of the resonant adhesion structure

The variation of the ARF with the thickness of the unit of the resonant adhesion structure is studied. As shown in Fig. 8, only when the frequency of the incident acoustic beam is 13 MHz, the resonant adhesion structure can obtain a negative ARF at an appropriate value of a_3 . This also provides a parametric dimension for the design of the units of the resonant adhesion structure. Compared with a_1 and a_2 , the influence of a_3 on the ARF is not very drastic. Therefore, the ARF changes more smoothly with a_3 . As can be seen from Fig. 2, the reversal of the ARF will only occur at an appropriate frequency. Therefore, when the incident frequency is 13 MHz, the negative ARF can be generated. However, under the action of higher or lower incident frequencies, the direction of the ARF does not reverse, which is also confirmed by the results of sound field distribution in Fig. 9. Similar to a_2 , the influence of a_3 on the ARF is more reflected in changing the boundary condition of the resonant cavity by changing the length of the emission aperture.

To illustrate the sound field distribution in more detail, the spatial distribution of the sound pressure is plotted as shown in Fig. 9. Figures 9(a)–9(c), respectively, show the sound pressure distribution

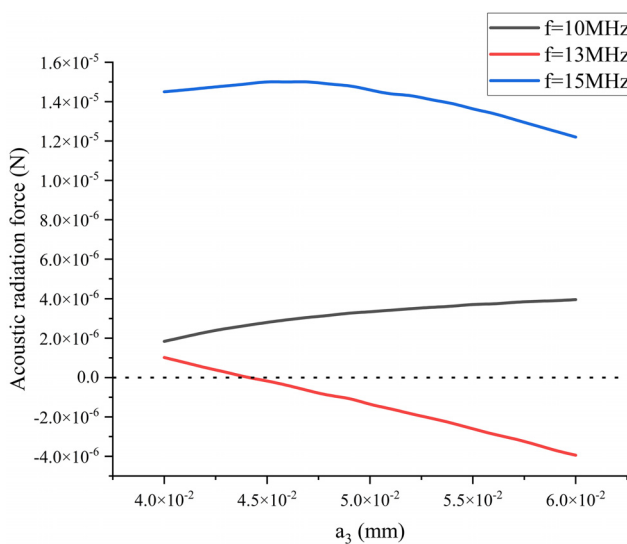


FIG. 8. Variation of the ARF with the thickness of the unit of the resonant adhesion structure.

when the thickness of the unit of the resonant adhesion structure is 0.04 mm and the incident sound wave frequency is 10, 13, and 15 MHz. With the impact of the incident sound waves of these three frequencies, the units of the resonant adhesion structure all experience forward ARFs. Figures 9(d)–9(f), respectively, depict the sound pressure distribution when the thickness of the unit of the resonant adhesion structure is 0.05 mm and the incident sound wave frequency is 10, 13, and 15 MHz. Only for the incident sound wave at the frequency of 13 MHz, the unit of the resonant adhesion structure is subject to a negative ARF. With the impact of the incident sound waves of the other two frequencies, the ARF applied to the unit of the resonant adhesion structure remains positive. Figures 9(g)–9(i), respectively, show the sound pressure distribution the thickness of the unit of the resonant adhesion structure is 0.06 mm and the incident sound wave frequency is 10, 13, and 15 MHz. Only for the incident sound wave at the frequency of 13 MHz, the unit of the resonant adhesion structure experiences a negative ARF. With the impact of the incident sound waves of the other two frequencies, the ARF experienced by the unit of the resonant adhesion structure remains positive. If the temperature changes to the volume is used to regulate the ARF affected by the unit, the thickness of the unit is a factor that cannot be ignored.

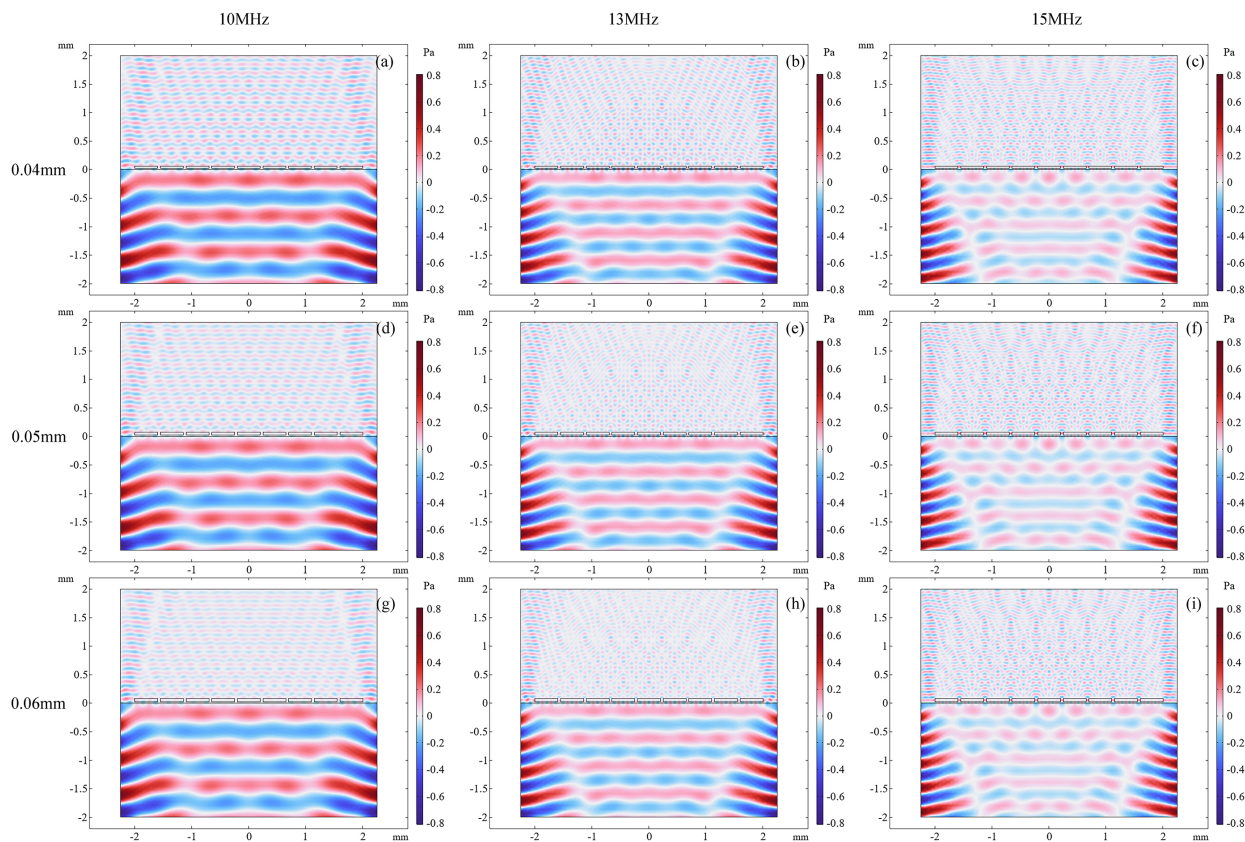


FIG. 9. Sound pressure distributions when the incident sound wave frequency and the thickness of the unit of the resonant adhesion structure are (a) 10 MHz, 0.04 mm; (b) 13 MHz, 0.04 mm; (c) 15 MHz, 0.04 mm; (d) 10 MHz, 0.05 mm; (e) 13 MHz, 0.05 mm; (f) 15 MHz, 0.05 mm; (g) 10 MHz, 0.06 mm; (h) 13 MHz, 0.06 mm; and (i) 15 MHz, 0.06 mm.

E. Variation law of acoustic radiation force with the width of the gap between the resonant adhesion structure and the auxiliary resonant structure

The variation of the ARF with the width of the gap between the resonant adhesion structure and the auxiliary resonant structure is studied, as shown in Fig. 10. It can be seen in Fig. 10(a) that when the resonant adhesion structure and the auxiliary resonant structure are very close ($a_4 < 0.01$ mm), the negative ARF appears under all frequency conditions. When the resonant adhesion structure and the auxiliary resonant structure are very close, each unit is affected by a negative ARF in the whole. When the resonant adhesion structure and the auxiliary resonant structure are very far away, the multiple scattering does not occupy a dominant role, so each unit is affected by a positive ARF in the whole. When the resonant adhesion structure and the auxiliary resonant structure are moderate, the units can be subject to a negative ARF under specific parameters.

Figure 10(b) is the enlarged image of Fig. 10(a). It can be seen that when the gap between the resonant adhesion structure and the auxiliary resonant structure is moderate, under a specific frequency condition 13 MHz, the resonant adhesive structure can still experience a negative ARF. When the distance between the resonant adhesion structure and the auxiliary resonant structure is very large, the resonant structure is destroyed, and the structure no longer features existence of obtaining a negative ARF.

To illustrate the sound field distribution in more detail, the spatial distribution of the sound pressure is plotted as shown in Fig. 11. Figures 11(a)–11(c), respectively, show the sound pressure distribution when the gap between the resonant adhesion structure and the auxiliary resonant structure is 0.001 mm and the incident sound frequency is 10, 13, and 15 MHz. It can be seen that the resonant adhesion structure experiences an obvious negative ARF. Figures 11(d)–11(f), respectively, depict the sound pressure distribution when the gap between the resonant adhesion structure and the auxiliary resonant structure is 0.01 mm and the frequency of the incident sound wave is 10, 13, and 15 MHz. With the impact of incident sound waves of these three

frequencies, the units of the resonant adhesion structure are still all subject to negative ARFs. Figures 11(g)–11(i), respectively, show the sound pressure distribution when the gap between the resonant adhesion structure and the auxiliary resonant structure is 0.02 mm and the incident sound wave frequency is 10, 13, and 15 MHz. Only for the incident sound wave at the frequency of 13 MHz, the unit of the resonant adhesion structure experiences a negative ARF. For the incident sound waves of the other two frequencies, the ARF experienced by the unit of the resonant adhesion structure has turned to the positive direction. Figures 11(j)–11(l), respectively, depict the sound pressure distribution when the gap between the resonant adhesion structure and the auxiliary resonant structure is 0.03 mm and the frequency of the incident sound wave is 10, 13, and 15 MHz. With the impact of the incident sound waves of these three frequencies, the units of the resonant adhesion structure are all subject to forward ARFs.

From the perspective of dynamics, there are two situations in the case of steady state: the distance between the resonant adhesion structure and the auxiliary resonant structure is infinitely long and the distance between the resonant adhesion structure and the auxiliary resonant structure is vanishing. When the interval between the resonant adhesion structure and the auxiliary resonant structure stays narrow, the negative ARF can provide schemes for picking devices which could transfer tiny objects.

IV. DISCUSSION AND CONCLUSION

As shown in Fig. 12, this design could have many interesting applications. In Fig. 12(a), resonant adhesion structure could be designed for screening and picking up in fluid media. Tiny objects can be picked up and positioned using a tip covered with the resonant adhesion structure. Based on the sensitivity of the direction of the acoustic radiation force to the parameters of the resonant adhesion structure, different specific binding resonant adhesion structures can be designed to specifically screen tiny objects. In Fig. 12(b), the frequency parameters can be modulated by the phased array, so it could be realized that some units are subject to negative acoustic radiation

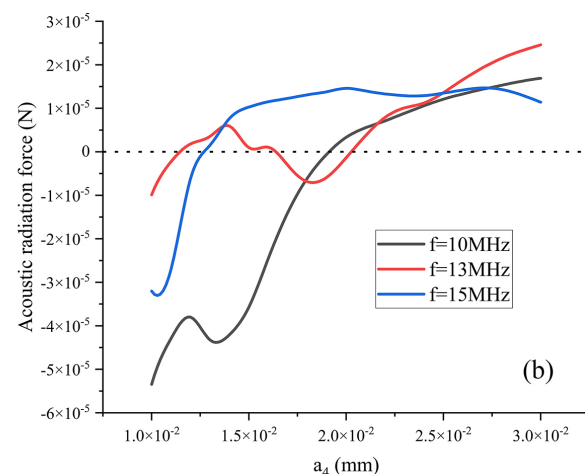
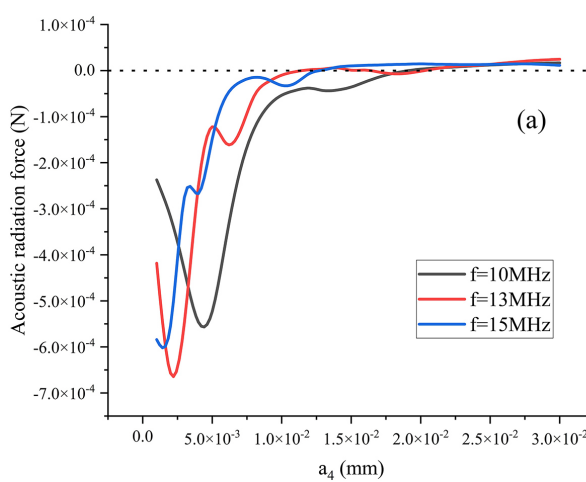


FIG. 10. (a) The variation of the ARF with the width of the gap between the resonant adhesion structure and the auxiliary resonant structure. (b) The enlarged image of the variation of the ARF with the width of the gap between the resonant adhesion structure and the auxiliary resonant structure.

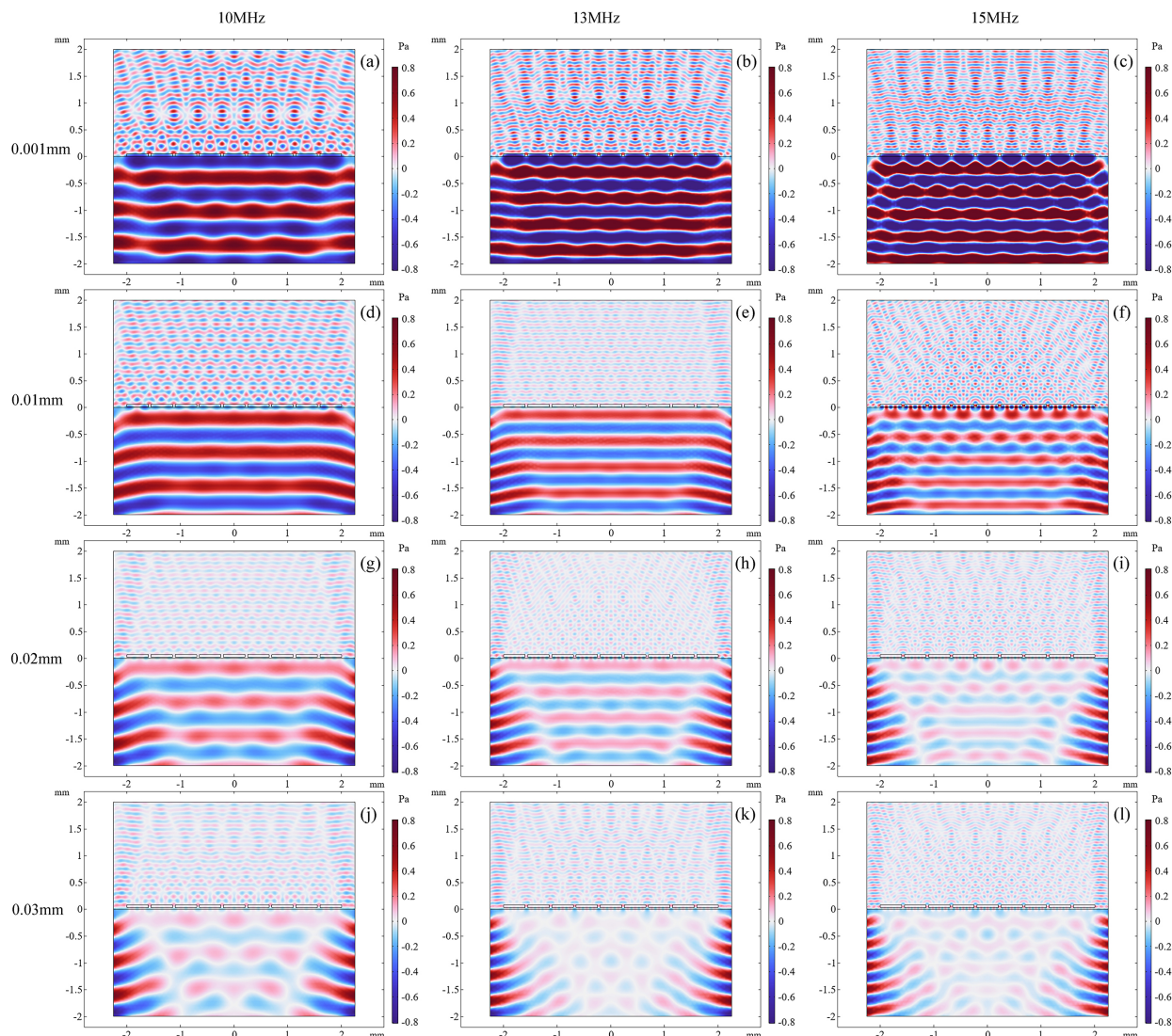


FIG. 11. The sound pressure distributions when the incident sound frequency and the gap between the resonant adhesion structure and the auxiliary resonant structure are (a) 10 MHz, 0.001 mm; (b) 13 MHz, 0.001 mm; (c) 15 MHz, 0.001 mm; (d) 10 MHz, 0.01 mm; (e) 13 MHz, 0.01 mm; (f) 15 MHz, 0.01 mm; (g) 10 MHz, 0.02 mm; (h) 13 MHz, 0.02 mm; (i) 15 MHz, 0.02 mm; (j) 10 MHz, 0.03 mm; (k) 13 MHz, 0.03 mm; and (l) 15 MHz, 0.03 mm.

Downloaded from http://pubs.aip.org/aip/phf/article-pdf/doi/10.1063/5.0150180/17359419057108_1.5.0150180.pdf

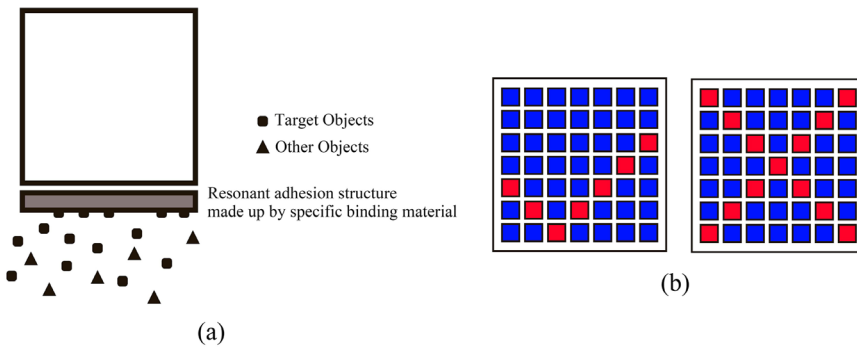


FIG. 12. Schematic diagram of applications of resonant adhesion structure.

force, while some units experience positive acoustic radiation force to construct an acoustic pixel display.

In this work, a new realization mechanism of negative acoustic radiation force is proposed, which is verified by finite element simulations. The variation law of the acoustic radiation force with the frequency of the incident acoustic beam and the parameters of the resonant adhesion structure is studied in detail. Various size parameters of the resonant structure can be adjusted to adapt to different incident frequency parameters. The width of the resonant cavity can be used to adjust the number and amplitude of the resonant peaks. The length and width of the emission aperture of the resonance cavity can adjust the radiation efficiency and boundary conditions of the resonance cavity. These parameters affect the inversion of the acoustic radiation force together. Because of the formation of the suitable resonant cavity, the special value of near-field multiple scattering makes the acoustic radiation force reversed. This design has broad application prospects in fields such as medicine and life sciences that urgently need precise controls.

ACKNOWLEDGMENTS

This project was supported by the National Key R&D program of China (No. 2020YFA0211400), the State Key Program of National Natural Science of China (No. 11834008), the National Natural Science Foundation of China (Nos. 12174192 and 12204119), the State Key Laboratory of Acoustics, Chinese Academy of Sciences (No. SKLA202210), and the Key Laboratory of Underwater Acoustic Environment, Chinese Academy of Sciences (No. SSHJ-KFKT-1701).

AUTHOR DECLARATIONS

Conflict of Interest

The authors have no conflicts to disclose.

Author Contributions

Menyang Gong: Conceptualization (lead); Data curation (lead); Formal analysis (lead); Investigation (lead); Methodology (lead); Project administration (lead); Resources (lead); Software (lead); Supervision (lead); Validation (lead); Visualization (lead); Writing – original draft (lead); Writing – review & editing (equal). **Minji Shi:** Conceptualization (supporting); Methodology (supporting); Writing – review & editing (supporting). **Yuanyuan Li:** Data curation (supporting). **Xin Xu:** Data curation (supporting). **Zhonghan Fei:** Data curation (supporting). **Yupei Qiao:** Data curation (supporting). **Jiehui Liu:** Methodology (supporting). **Aijun He:** Methodology (supporting). **Xiaozhou Liu:** Funding acquisition (lead); Project administration (supporting); Resources (supporting); Supervision (supporting); Writing – review & editing (equal).

DATA AVAILABILITY

The data that support the findings of this study are available from the corresponding authors upon reasonable request.

REFERENCES

- ¹S. Deshmukh, Z. Brzozka, T. Laurell, and P. Augustsson, "Acoustic radiation forces at liquid interfaces impact the performance of acoustophoresis," *Lab Chip* **14**, 3394–3400 (2014).
- ²C. Goering and J. Dual, "Measuring the effects of a pulsed excitation on the buildup of acoustic streaming and the acoustic radiation force utilizing an optical tweezer," *Phys. Rev. E* **105**, 055103 (2022).
- ³J. Y. Gu, L. F. Du, M. Bai, H. L. Chen, X. Jia, J. Zhao, and X. M. Zhang, "Preliminary study on the diagnostic value of acoustic radiation force impulse technology for differentiating between benign and malignant thyroid nodules," *J. Ultrasound Med.* **31**, 763–771 (2012).
- ⁴M. Rajabi and A. Mojahed, "Acoustic manipulation of oscillating spherical bodies: Emergence of axial negative acoustic radiation force," *J. Sound Vib.* **383**, 265–276 (2016).
- ⁵M. Tozaki, S. Isobe, and E. Fukuma, "Preliminary study of ultrasonographic tissue quantification of the breast using the acoustic radiation force impulse (arf) technology," *Eur. J. Radiol.* **80**, E182–E187 (2011).
- ⁶S. Z. Hoque and A. K. Sen, "Interparticle acoustic radiation force between a pair of spherical particles in a liquid exposed to a standing bulk acoustic wave," *Phys. Fluids* **32**, 072004 (2020).
- ⁷H. O. Caldag and S. Yesilyurt, "Acoustic radiation forces on magnetically actuated helical swimmers," *Phys. Fluids* **32**, 092012 (2020).
- ⁸S. Xue, X. W. Zhang, F. He, Z. M. Liu, and P. F. Hao, "Acoustic particle migration and focusing in a tilted acoustic field," *Phys. Fluids* **33**, 122006 (2021).
- ⁹A. Dolev, M. Kaynak, and M. S. Sakar, "Dynamics of entrapped microbubbles with multiple openings," *Phys. Fluids* **34**, 012012 (2022).
- ¹⁰A. Pavlic, P. Nagpure, L. Ermanni, and J. Dual, "Influence of particle shape and material on the acoustic radiation force and microstreaming in a standing wave," *Phys. Rev. E* **106**, 015105 (2022).
- ¹¹T. Q. Tang and L. X. Huang, "An efficient semi-analytical procedure to calculate acoustic radiation force and torque for axisymmetric irregular bodies," *J. Sound Vib.* **532**, 117012 (2022).
- ¹²T. Q. Tang, G. T. Silva, L. X. Huang, and X. Han, "Acoustic levitation of axisymmetric Mie objects above a transducer array by engineering the acoustic radiation force and torque," *Phys. Rev. E* **106**, 045108 (2022).
- ¹³H. Tanaka, K. Funayama, and Y. Tadokoro, "Periodic switching of acoustic radiation force with beat created by multitone field," *Sci. Rep.* **12**, 15029 (2022).
- ¹⁴M. W. Urban, "Production of acoustic radiation force using ultrasound: Methods and applications," *Expert Rev. Med. Devices* **15**, 819–834 (2018).
- ¹⁵H. B. Wang, S. Gao, Y. P. Qiao, J. H. Liu, and X. Z. Liu, "Theoretical study of acoustic radiation force and torque on a pair of polymer cylindrical particles in two Airy beams fields," *Phys. Fluids* **31**, 047103 (2019).
- ¹⁶H. B. Wang, Y. P. Qiao, J. H. Liu, B. Jiang, G. T. Zhang, C. W. Zhang, and X. H. Liu, "Experimental study of the difference in deformation between normal and pathological, renal and bladder, cells induced by acoustic radiation force," *Eur. Biophys. J.* **49**, 155–161 (2020).
- ¹⁷Q. Wang, A. Riaud, J. Zhou, Z. X. Gong, and M. Baudoin, "Acoustic radiation force on small spheres due to transient acoustic fields," *Phys. Rev. Appl.* **15**, 044034 (2021).
- ¹⁸S. G. Zhao, M. X. Wu, S. J. Yang, Y. Q. Wu, Y. Y. Gu, C. Y. Chen, J. Ye, Z. M. Xie, Z. H. Tian, H. Bachman, P. H. Huang, J. P. Xia, P. R. Zhang, H. Y. Zhang, and T. J. Huang, "A disposable acoustofluidic chip for nano/microparticle separation using unidirectional acoustic transducers," *Lab Chip* **20**, 1298–1308 (2020).
- ¹⁹P. L. Marston and D. B. Thiessen, "Manipulation of fluid objects with acoustic radiation pressure," *Transp. Phenom. Microgravity* **1027**, 414–434 (2004).
- ²⁰P. L. Marston, W. Wei, and D. B. Thiessen, "Acoustic radiation force on elliptical cylinders and spheroidal objects in low frequency standing waves," *Innovations Nonlinear Acoust.* **838**, 495–499 (2006).
- ²¹M. L. Palmeri and K. R. Nightingale, "Acoustic radiation force-based elasticity imaging methods," *Interface Focus* **1**, 553–564 (2011).
- ²²Y. P. Qiao, M. Y. Gong, H. B. Wang, J. Lan, T. Liu, J. H. Liu, Y. W. Mao, A. J. He, and X. Z. Liu, "Acoustic radiation force on a free elastic sphere in a viscous fluid: Theory and experiments," *Phys. Fluids* **33**, 047107 (2021).
- ²³Y. P. Qiao, H. B. Wang, X. Z. Liu, and X. F. Zhang, "Acoustic radiation force on an elastic cylinder in a Gaussian beam near an impedance boundary," *Wave Motion* **93**, 102478 (2020).
- ²⁴Y. P. Qiao, X. W. Zhang, M. Y. Gong, H. B. Wang, and X. Z. Liu, "Acoustic radiation force and motion of a free cylinder in a viscous fluid with a boundary defined by a plane wave incident at an arbitrary angle," *J. Appl. Phys.* **128**, 044902 (2020).

- ²⁵A. Alhyari, C. Gorg, C. F. Dietrich, C. Trenker, M. Ludwig, and E. S. Zadeh, "Diagnostic performance of point shear wave elastography using acoustic radiation force impulse technology in peripheral pulmonary consolidations: A feasibility study," *Ultrasound Med. Biol.* **48**, 778–785 (2022).
- ²⁶Z. X. Gong, P. L. Marston, and W. Li, "T-matrix evaluation of three-dimensional acoustic radiation forces on nonspherical objects in bessel beams with arbitrary order and location," *Phys. Rev. E* **99**, 063004 (2019).
- ²⁷W. Wei, D. B. Thiessen, and P. L. Marston, "Acoustic radiation force on a compressible cylinder in a standing wave," *J. Acoust. Soc. Am.* **116**, 201–208 (2004).
- ²⁸R. R. Wu, K. X. Cheng, X. Z. Liu, J. H. Liu, X. F. Gong, and Y. F. Li, "Study of axial acoustic radiation force on a sphere in a Gaussian quasi-standing field," *Wave Motion* **62**, 63–74 (2016).
- ²⁹L. K. Zhang and P. L. Marston, "Acoustic radiation force expressed using complex phase shifts and momentum-transfer cross sections," *J. Acoust. Soc. Am.* **140**, El178–El183 (2016).
- ³⁰M. Y. Gong, X. Xu, Y. P. Qiao, Z. H. Fei, Y. Y. Li, J. H. Liu, A. J. He, and X. Z. Liu, "Scheme of non-contact manipulation: Acoustic radiation force on spherical particle in a spherical shell structure," *Results Phys.* **46**, 106264 (2023).
- ³¹M. Y. Gong, Y. P. Qiao, Z. H. Fei, Y. Y. Li, J. H. Liu, Y. W. Mao, A. J. He, and X. Z. Liu, "Non-diffractive acoustic beams produce negative radiation force in certain regions," *AIP Adv.* **11**, 065029 (2021).
- ³²M. Y. Gong, Y. P. Qiao, J. Lan, and X. Z. Liu, "Far-field particle manipulation scheme based on x wave," *Phys. Fluids* **32**, 117104 (2020).
- ³³M. Rajabi and A. Mojahed, "Acoustic radiation force control: Pulsating spherical carriers," *Ultrasonics* **83**, 146–156 (2018).
- ³⁴H. Q. Yu, J. Yao, D. J. Wu, X. W. Wu, and X. J. Liu, "Negative acoustic radiation force induced on an elastic sphere by laser irradiation," *Phys. Rev. E* **98**, 053105 (2018).
- ³⁵D. Baresch, J. L. Thomas, and R. Marchiano, "Three-dimensional acoustic radiation force on an arbitrarily located elastic sphere," *J. Acoust. Soc. Am.* **133**, 25–36 (2013).
- ³⁶S. Y. Li, J. Y. Shi, and X. F. Zhang, "Study on acoustic radiation force of an elastic sphere in an off-axial Gaussian beam using localized approximation," *J. Acoust. Soc. Am.* **151**, 2602–2612 (2022).